Separation and Purification Technology 320 (2023) 124115

Contents lists available at ScienceDirect

Separation and Purification Technology

journal homepage: www.elsevier.com/locate/seppur

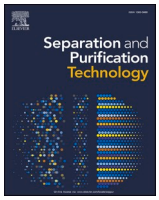

Polymer/ionic liquid pilot scale membrane prototype for the recovery of difluoromethane (R-32) from refrigerant mixtures

Fernando Pardo, Sergio V. Gutiérrez-Hernández, Paula Rodríguez-San Miguel, Gabriel Zarca *, Ane Urtiaga *

Department of Chemical and Biomolecular Engineering, University of Cantabria, Av. Los Castros 46, Santander 39005, Spain

ARTICLE INFO

Keywords:
Thin film composite
Spray coating
Fluorinated hydrocarbon
Gas separation
Scale-up
Pebax membrane

ABSTRACT

Difluoromethane (R-32) is a hydrofluorocarbon (HFC) that has been massively used over the last 30 years in refrigeration and air conditioning as a primary component of azeotropic or close boiling refrigerant mixtures. Despite environmental directives commanded to drastically reduce the use of HFCs, R-32 has excellent thermodynamic properties and moderate GWP, thus its recovery from depleted mixtures collected from end-of-life equipment is sought to synthesize alternative low-GWP refrigerant blends. Membrane separation using composite polymer/ionic liquid membranes based on poly-ether-block-amide have shown potential to separate R-32 from other fluorinated hydrocarbons, yet the development of this type of composite membranes still remains at laboratory scale. In this work, a spray coating technique was successfully applied to create defect-free thin selective layers of neat Pebax®1657, Pebax®1657/40 wt% $[C_2C_1im][BF_4]$ and Pebax®1657/40 wt% $[C_2C_1im]$[SCN] coated on porous PVDF substrates. This methodology was transferred from the lab-scale tests (12.6 cm^2) to a custom pilot set-up (300 cm^2). The pilot results confirmed the superior performance and stability of $[C_2C_1im]$[SCN]-based membranes, which allowed the recovery of up to 64.3% and 67.1% R-32 from the refrigerant mixtures R-410A (69.8 mol % R-32 and 30.2 mol % R-125) and R-454B (82.1 mol % R-32 and 17.9 mol % R-1234yf) at 6 bar, increasing the R-32 permeate concentration up to 89.6 and 95.9 mol %, respectively. These results highlight the need to expand the knowledge of this type of gas separation membranes towards thinner and defect-free selective dense layers with the purpose of approaching their real applications.

1. Introduction

With the demand for refrigeration and air-conditioning (RAC) continuously growing as a consequence of global warming and increased wealth and population in tropical regions [1,2], great interest has arisen in recovering exhausted refrigerants from end-of-life equipment with the aim of recycling the most valuable compounds [3]. To date, most working fluids used as refrigerants in vapor-compression cycles consist of mixtures of fluorinated hydrocarbons that aim to balance the intricate trade-offs between environment, health and safety [4]. In the current scenario, hydrofluorocarbon (HFC) mixtures have been widely used because of their null ozone depletion potential and excellent thermodynamic performance. However, with the ratification of the Kigali Amendment to the Montreal Protocol, a new regulatory roadmap (e.g., European Regulation 517/2014, U.S. Bill S.2754) was set to drastically reduce the manufacture and marketing of HFCs due to their contribution to global warming. Under this scenario, some HFCs are being substituted by hydrofluoroolefins (HFOs), another family of fluorinated compounds that exhibit negligible global warming potential (GWP), good thermodynamic performance and low flammability [5]. Consequently, it is expected that mixtures of low-GWP HFOs and moderate-GWP HFCs will become predominant refrigerant fluids in commercial, stationary and industrial refrigeration [6]. A distinguishing feature of HFCs and HFC/HFO refrigerant blends is that they usually exhibit azeotropic or near-azeotropic behavior that provides them with better refrigeration performance [7]. This characteristic, however, poses a challenge for the separation of their individual constituents by conventional distillation [8]. In this regard, recent literature reports the progress towards advanced separation processes like extractive distillation using ionic liquids (ILs) as entrainers [9–15], and adsorption in carbon [16], zeolites [17], MOFs [1,18,19] and other porous materials [20]. In addition, the separation of refrigerant mixtures with membrane technology is also

* Corresponding authors.
E-mail addresses: zarcag@unican.es (G. Zarca), urtiaga@unican.es (A. Urtiaga).

https://doi.org/10.1016/j.seppur.2023.124115
Received 31 January 2023; Received in revised form 29 April 2023; Accepted 14 May 2023
Available online 19 May 2023

Table 1
Name, molecular structure and molar volume (V_m, at 30 °C and 1 bar) of ILs used in Pebax®-based CILPMs [23].

IL	Name	Cation	Anion	CAS No.	V_m ($cm^3 \cdot mol^{-1}$)
$[C_2mim][SCN]$	1-Ethyl-3-methylimidazolium thiocyanate			331717–63-6	151.9
$[C_2mim][BF_4]$	1-Ethyl-3-methylimidazolium tetrafluoroborate		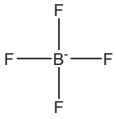	143314–16-3	154.8
$[C_2mim][OTf]$	1-Ethyl-3-methylimidazolium triflouromethanesulfonate	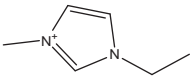	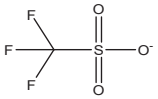	145022–44-2	188.3
$[C_2mim][Tf_2N]$	1-Ethyl-3-methylimidazolium bis(trifluoromethylsulfonyl) imide		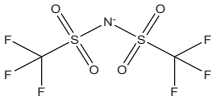	174899–82-2	258.5

Table 2
Summary of gas separations with IL-containing thin film composite membranes (TFCMs). n.a.: not available. Table S1 of the SI presents the chemical name and CAS number of the ILs included in this table.

Selective layer				Support (pore size), filler and configuration (area)	Gutter/ Protective layer	Technique	Separation	Ref.
Polymer	IL (see Table S1)	IL content (wt %)	δ (μm)					
Poly(IL)	$[C_2C_1im][Tf_2N]$	58	0.1	(n.a.), flat (10.2 cm rectangular support)	3M® proprietary	casting line	CO_2/N_2	[35]
Pebax®2533	$[TETA][CF_3CO_2]$	30	0.2–0.5	PSf (20 kDa), flat (n.a.)	PDMS	dip coating	CO_2/N_2	[36]
Pebax®1657	$[C_2C_1im][BF_4]$	20–80	1–2	PVDF (0.5 μm), flat (9.6 cm^2) and hollow fiber (12.3 cm^2)	PTMSP	dip coating	CO_2/N_2, CO_2/CH_4	[31]
Poly(IL)	$[Pyrr_{14}][Tf_2N]$	25–40	3–10	PI (n.a.), flat discs (2.1 and 13.1 cm^2)	PDMS	ultrasonic coating	CO_2/N_2	[37]
Polyamide	$[C_2C_1im][Tf_2N]$	0–5	–	PSf (n.a.), flat (n.a.)	none	interfacial polymerization	CO_2/CH_4	[38]
PVP – Nafion	$[C_6C_1im][BF_4]$ $[C_6C_1im][PF_6]$	11.3 – 12.0 mmol/g % PVP 33.8 – 35.7 mmol/g % PVP/Nafion	–	PSf (70 nm), flat (n.a.)	none	polymer-support (electrospinning) polymer-IL (impregnation)	CO_2/CH_4	[39]
PIM-1	$[C_4C_1im]_2[Co(SCN)_4]$	0.4–2	0.5–0.6	PAN (20 kDa), flat (n.a.)	none	dip-coating	O_2/N_2	[40]
Pebax®1657	[APMim][Br]	0.01–0.5	0.1	PAN (n.a.), Graphene oxide, flat (n.a.)	PTMSP	casting-solution	CO_2/N_2, CO_2/H_2	[41]
Pebax®1657	[DnBM][Cl]	38–42	0.76–1.14	Macroporous PC (894 nm), flat (n.a.)	none	inclined-coating	$CO_2/N_2/CH_4$	[42]
Pebax®1657	$[C_2C_1im][BF_4]$	20–50	2.9–6.4	PSf (n.a.), flat (15.9 cm^2)	none	co-casting	$CO_2/N_2/CH_4$	[43]

Polymers: Poly(IL): Polymerized Ionic liquid, PVP: Polyvinylpyrrolidone, PIM: Polymer of intrinsic microporosity, PSf: Polysulfone, PI: Polyimide, PVDF: Polyvinylidene fluoride, PAN: Polyacrylonitrile, PDMS: Polydimethylsiloxane, PTMSP: Poly(1-trimethylsilyl-1-propyne), PC: Polycarbonate.

receiving increasing attention, yet only a few type of polymers have been tested as thick membranes based on different poly(ether-block-amide) copolymers (PEBA) [21–25], perfluoro(butenyl vinyl ether) and perfluoro(2,2-dimethyl-1,3-dioxole) copolymers (PBVE:PDD) [26,27], and polymers of intrinsic microporosity (PIM-1) [28]. A comparison between the separation performance of these membranes can be found in the latter work [28]. Beyond polymer membranes, the engineering of composite ionic liquid polymer membranes (CILPMs) appeared as a powerful approach to enhance gas permeability and selectivity in challenging separations of binary refrigerant mixtures (namely, R-410A, R-454B and R-513A) [21–23,25], similarly to that exhibited in CO_2/N_2 and CO_2/CH_4 separations [29,30]. In these works, the thermoplastic copolymer poly(ether-*block*-amide) demonstrated outstanding compatibility with several ILs, resulting in composite polymer/IL membranes with improved permeability and selectivity properties, in which the main role of the IL contained within the polymer matrix was to modify the solubility of the gases in the composite films. In this context, CILPMs prepared with fluorinated ILs such as $[C_2C_1im][Tf_2N]$, $[C_2C_1im][OTf]$ and $[C_2C_1im][BF_4]$ (Table 1) notably increased the permeability of fluorinated refrigerants, yet only the CILPMs containing small molar volume ILs exhibited significantly higher selectivity than the neat Pebax 1657 polymer. In particular, CILMPs containing 40 wt% $[C_2C_1im][BF_4]$ or $[C_2C_1im][SCN]$ showed the best gas separation performance and mechanical stability against feed pressure [23,25].

However, the selection of the best IL candidates is not the whole story. Most polymer/IL membranes are tested as self-supported thick dense films (>50 μm) that are not attractive for an industrial application. Instead, these IL-based membranes should be processed into defect-free thin films, in order to provide high gas permeance, and conveniently packed. Yet, the production of thin film composite membranes (TFCMs) containing free IL is still a quite unexplored field of research. Table 2 shows a summary of the IL-containing TFCMs reported up to date to the best of our knowledge. In all cases, the TFCMs were prepared as multilayer composite membranes using a porous support above which the selective layer, a blend of either polymer/IL or poly(IL)/IL, was casted by different coating techniques. The final thickness of the selective layer ranged between 0.1 μm and a few micrometers. In addition, highly permeable polymers such as rubbery PDMS and glassy PTMSP

were used as gutter layer and/or protective layer. Regarding the membrane configuration, only Fam et al. [31] fabricated hollow fiber membranes, whereas the other authors reported flat membranes. As can be seen, none of the reported membrane areas exceeded 16 cm^2, thus upscaling this type of composite materials still remains as a major objective in order to evaluate their reliability and whether they can be considered a real alternative for gas separations. Overall, the question remains as whether IL-containing TFCMs can outperform polymer TFCMs in terms of gas permeance, selectivity and long-term performance. In addition, all of these IL-containing TFCMs targeted the separation of CO_2 from either N_2 or CH_4.

While detailed studies of polymer-coated TFCMs that evaluate the separation performance of membrane modules at pilot plant scale are common [32,33], the scale up of IL-based TFCMs for gas separation at large scale has not been addressed yet to the best of our knowledge. Thus, in this work, we aim to take a step forward in the separation of azeotropic and close-boiling mixtures of fluorinated hydrocarbons by fabricating polymer and polymer/IL TFCMs with a simple and reliable spray coating technique [34], which facilitates the deposition of a thin dense layer of the selective material on a substrate, minimizing penetration into the porous structure by rapid evaporation of the solvent. Another great advantage of spray coating is that it can be easily adapted to different types of geometry and larger dimensions of flat sheet membranes. And eventually, this work addresses for the first time the separation at pilot plant scale of two commercial refrigerant mixtures under relevant conditions of pressure and without sweep gas with the best TFCMs previously tested at lab-scale.

2. Experimental

2.1. Materials

Poly(ether-*block*-amide) (Pebax®1657MH grade) was kindly provided in pellets by Arkema. 1-ethyl-3-methylimidazolium tetrafluoroborate (purity > 98%) [C_2C_1im][BF_4] and 1-ethyl-3-methylimidazolium-thiocyanate (purity > 98 %) [C_2C_1im][SCN] were purchased from Sigma-Aldrich and IoLiTec, respectively. Hydrophobic microporous PVDF flat discs (0.2 μm pore size, 70% porosity, Pall Corporation) and roll transfer (0.2 μm pore size, Thermo Scientific) were selected as supports. Refrigerant gases were tested either as pure gases (difluoromethane (R-32), 1,1,1,2-tetrafluoroethane (R-134a), 2,3,3,3-tetrafluoropropene (R-1234yf)), or as gas mixtures, namely, R-410A (50:50 wt% R-32 and R-125) and R-454B (69.9:31.1 wt% R-32 and R-1234yf). Table S2 of the Supporting Information (SI) summarizes the main properties of the F-gases used in this work. All materials were used as received. Ethanol (Scharlab) was the solvent used for preparing the polymer and polymer − IL casting solutions.

2.2. Membranes preparation

Thick dense membranes were prepared following the procedure described in our previous works and shown in Figure S1 (Supporting Information) [22–24]. Figure S1 also summarizes the spray coating methodology that was used to fabricate TFCMs made of Pebax®1657 following a similar procedure to that reported by Jiang et al. [34]. To that end, 3 wt% of Pebax 1657 beads were dissolved in 70:30 wt% ethanol/water under magnetic stirring at 70 °C for 24 h. Afterwards, for the Pebax®1657/IL TFCMs, the IL was added to the polymer solution at a polymer:IL ratio of 60:40 wt%, and stirred for 2 h. The PVDF microfiltration supports were cut and inserted between two stainless steel plates provided with window sizes equivalent to the desired effective membrane areas, circular-shaped 12.6 cm^2 for the lab-scale membranes and rectangular-shaped 150 cm^2 for the pilot scale membranes. The whole assembly was placed over a hotplate at 70 °C to enable fast solvent evaporation and avoid polymer intrusion into the pores of the support. Eventually, the solution was sprayed using an airbrush (0.4 mm nozzle, Harder & Steenbeck Colani) in consecutive layers, turning the assembly 90° each time to obtain a homogenous film. To assess the influence of membrane thickness, TFCMs were sprayed either four or eight times. The trials performed to further reduce the number of 4 spray-coated layers resulted in membranes that did not withstand operation pressures above 8.5 bar. The final weight of the selective layer, determined by weight difference with respect to the support, was 10–20 mg of polymer or polymer/IL in the lab-scale, and 500–600 mg in the pilot scale membranes. Table 3 presents the whole set of membranes prepared in this work, which includes two thick membranes prepared with the conventional solvent casting methodology (***M1*** and ***M4***), and different thin film membranes prepared with the spray coating technique using both neat Pebax®1657 and blends of Pebax®1657 with 40 wt% IL. Four of them were fabricated in the lab-scale size by spraying either 8 coating layers (***M2***, ***M5***) or 4 coating layers (***M3***, ***M6***), and three of them in the pilot scale size with 4 coating layers (***M7*** to ***M9***).

Table 3
List of membranes prepared in this work.

Code	Membrane type and selective layer	Casting technique	Area (cm^2)	Number of coating layers	Dense layer thickness (μm)
M1	Neat Pebax®1657	solvent evaporation	12.6	–	63
M2	TFCM-Neat Pebax®1657	spray-coating		8	9.0
M3	TFCM-Neat Pebax®1657	spray-coating		4	5.4
M4	Pebax®1657/40 wt% [C_2C_1im][BF_4]	solvent evaporation		–	60
M5	TFCM-Pebax®1657/40 wt% [C_2C_1im][BF_4]	spray-coating		8	38
M6	TFCM-Pebax®1657/40 wt% [C_2C_1im][BF_4]	spray-coating		4	15.5
M7	TFCM-Neat Pebax®1657	spray-coating	150	4	10
M8	TFCM-Pebax®1657/40 wt% [C_2C_1im][BF_4]	spray-coating		4	8.8
M9	TFCM-Pebax®1657/40 wt% [C_2C_1im][SCN]	spray-coating		4	9.3

2.3. Membrane characterization

The morphology of the TFCM surface and cross section was characterized using scanning electron microscopy (SEM, Carl Zeiss EVO MA 15). The samples were prepared by freeze-fracturing in liquid nitrogen followed by deposition of a gold thin film using a sputter coater (Balzers Union SCD040). Moreover, the Fourier transform infrared spectra (FT-IR) of the TFCMs were obtained with the attenuated total reflection (ATR) technique at room temperature (wavelength range 400–4000 cm^{-1}) in a FT-IR Spectrum 65 (Perkin Elmer, Italy).

2.4. Gas permeation

The gas separation performance of the lab-scale membranes was assessed in a custom-made stainless-steel permeation cell (8 cm diameter) which allows to operate with flat circular membranes of 12.6 cm^2 [22–25]. All experiments were performed at 30 °C feeding the pure gases or gas mixtures in continuous flow at 20 cm^3_{STP} min^{-1}. A back-pressure transducer allowed controlling the gas pressure (1.3 – 9.5 bar) at the feed side. An argon stream (4 cm^3_{STP} min^{-1}) swept the permeate

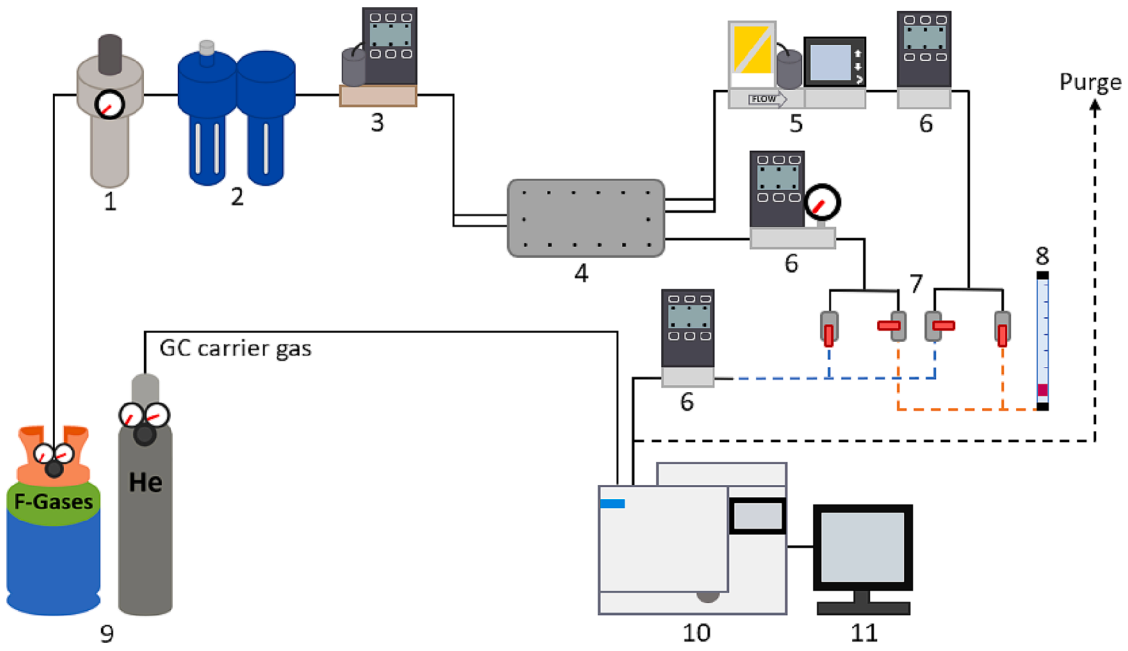

Fig. 1. Schematic design of the pilot plant system and the equipment. (1) Pressure regulator, (2) 0.1 and 1 μm coalescence filters, (3) feed stream mass flow controller, (4) membrane cell, (5) backpressure regulator, (6) retentate, permeate and GC-inlet mass flow meters and pressure indicators, (7) valves, (8) low range bubble flowmeter, (9) gas cylinders, (10) GC-TCD, (11) PC. Figure S3 (Supplementary material) magnifies the description of the pilot scale membrane test cell.

side of the membrane, and a gas chromatograph (Agilent 490 micro GC) equipped with a Pora Plot U column and a thermal conductivity detector (TCD) analyzed the permeate gas composition.

The scale-up study was performed in an experimental setup specially designed for continuous operation (Fig. 1). The pilot plant membrane module (17.5 cm length × 15 cm width) has rectangular-shaped housing and enables the insertion of two flat membranes (13.5 × 11.1 cm), which are placed in parallel at both sides of a porous sintered stainless-steel plate, resulting in an effective permeation area of 300 cm^2. The TFCMs membranes were sealed with flat Viton^{TM} rings and screwed with the shell part of the permeation cell (see the detailed graphical description in Figures S2 and S3 of the SI). The membrane module had two-inlet channels for the feed gas (50 cm^3_{STP} min^{-1}) and two outlet channels for the retentate stream. Accordingly, the transmembrane flux was stablished through both membranes generating a single permeate stream that exited the module through the central part of the shell. Note that the pressure on the permeate side of both the lab-scale and the pilot-scale membrane modules was the atmospheric pressure.

A mass flow controller (Omega FMA-LP2618A-I) supplied a constant feed flowrate of the commercial refrigerant mixture. Mass flow meters (Omega FMA-1618A) measured the flow rate at the outlet of the membrane cell (permeate and retentate streams) and a back-pressure regulator (Bronkhorst EL-PRESS P-702CV P1-control) controlled the upstream gas pressure. Pressure gauges were installed at the feed inlet and the permeate outlet. In addition, a bubble flowmeter was used to check flowrates below the measurable range of the mass flowmeters, thus enabling the verification of mass balances. The steady-state gas concentration in the permeate and retentate streams was measured online by a gas chromatograph (Agilent 8860 GC) equipped with a GC-Gas Pro column (60 m and 320 μm i.d.) and a thermal conductivity detector (TCD). Table S3 of the SI details the analytical method. In this work, all pilot scale experiments were performed at room temperature, 20 ± 1 °C, by feeding refrigerant mixtures (either R-410A or R-454B) at several feed pressures (1.5–6 bar). It is worth noting that a sweep gas stream was not used in the pilot experiments.

Gas permeability ($\mathscr{P}_i$) of the membranes, expressed in barrer units ($1\ \text{barrer} = 10^{-10}\ cm^3_{STP}\cdot cm\cdot cm^{-2}\cdot s^{-1}cmHg^{-1}$), was calculated according to Eq. (1)

$$\mathscr{P}_i = \frac{Q_i \cdot \delta}{A \cdot \left(\widehat{f}_{R,i} - \widehat{f}_{P,i}\right)} \tag{1}$$

where $Q_i\left(cm^3_{STP}\cdot s^{-1}\right)$ is the transmembrane flow of component i, $A(cm^2)$ is the membrane area, $\widehat{f}_{R,i}$ and $\widehat{f}_{P,i}(cmHg)$ are the mixed-gas fugacity of component i in the retentate and permeate streams, respectively, and $\delta(cm)$ is the membrane thickness. In addition, gas permeance $(\mathscr{P}_i/\delta)$ was also calculated for the TFCMs and expressed in gas permeation units $\left(1\ \text{GPU} = 10^{-6}\ cm^3_{STP}\cdot cm^{-2}\cdot s^{-1}cmHg^{-1}\right)$.

The component fugacity in the mixture was calculated as

$$\widehat{f}_i = \widehat{\varnothing}_i \cdot p_i \tag{2}$$

where $\widehat{\varnothing}_i$ is the mixed-gas fugacity coefficient of component i, which was determined using the REFPROP property method of Aspen Plus, and p_i is the partial pressure.

The separation performance was evaluated in terms of ideal gas pair selectivity for the pure gases,

$$\alpha_{i/j} = \frac{\mathscr{P}_i}{\mathscr{P}_j} \tag{3}$$

where i and j are the pure permeance of the most and least permeable gases, respectively. Whereas in experiments dealing with mixed gas permeation, the separation factor was calculated as,

$$SF_{i/j} = \frac{y_i/y_j}{x_i/x_j} \tag{4}$$

where y and x are the mole fraction composition in the permeate and feed streams, respectively. In this context, the separation factor is influenced by process variables such as the transmembrane pressure and the feed flowrate, among others, and by the intrinsic properties of the membrane material.

For the evaluation of the pilot plant performance, the following indicators were determined: R-32 purity (mol %) in the permeate stream, which was directly measured from GC/TCD analysis, R-32 recovery (%) (Eq. (5)), and the stage cut (Eq. (6)),

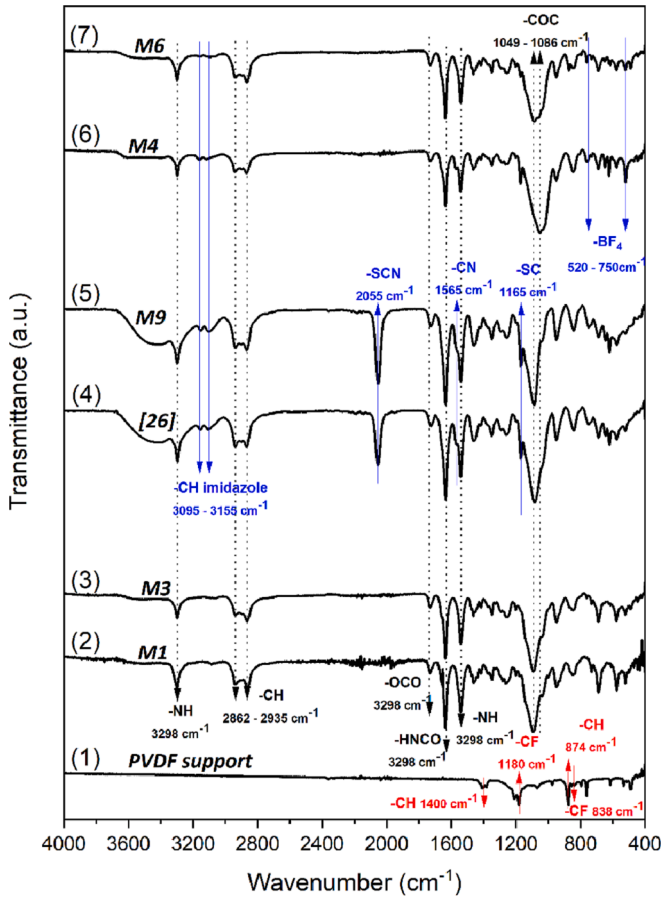

Fig. 2. FTIR spectra of Pebax, CILPM and IL-based TFCM. (1) PVDF support, (2) Neat Pebax (***M1***), (3) Neat Pebax TFCM (***M3***), (4) Pebax 1657-[C_2C_1im][SCN] (40 wt%) CILPM [25], (5) Pebax 1657-[C_2C_1im][SCN] (40 wt%) TFCM (***M9***), (6) Pebax 1657-[C_2C_1im][BF_4] (40 wt%) CILPM (***M4***), (7) Pebax 1657-[C_2C_1im][BF_4] (40 wt%) TFCM (***M6***). Blue line (IL bands), red line (PVDF bands), black dotted lines (Pebax bands).

$$Recovery_{R-32}(\%) = \frac{Q_{R-32}^{permeate}}{Q_{R-32}^{feed}} x100 = \frac{Q^{permeate} \cdot x_{R-32}^{permeate}}{Q^{feed} \cdot x_{R-32}^{feed}} x100 \quad (5)$$

$$Stagecut(\%) = \frac{Q^{permeate}}{Q^{feed}} x100 \quad (6)$$

where $Q_{R-32}^{permeate}$, Q_{R-32}^{feed}, $Q^{permeate}$, Q^{feed} are the R-32 and total flowrates ($cm_{stp}^3 \cdot min^{-1}$) in the permeate and feed streams, respectively. $x_{R-32}^{permeate}$ and x_{R-32}^{feed} stand for the molar composition of R-32 in the permeate and feed streams, respectively.

3. Results and discussion

3.1. FTIR characterization of Pebax®1657/IL-TFCMs

Fig. 2 shows the FTIR spectra of the support, the thick membranes and the TFCMs. The representative peaks of the PVDF support at 1400 cm^{-1} and 874 cm^{-1} were attributed to the bending and wagging vibration of the bond C–H. Additionally, the peaks observed at 1180 cm^{-1} and 838 cm^{-1} were assigned to C-F stretching and bending vibration, respectively [44]. On the other hand, the characteristic peaks of the neat Pebax 1657 membrane ***M1*** were attributed to N–H stretching and N–H bending vibrations at 3298 and 1539 cm^{-1}, respectively, the -O-C=O at 1735 cm^{-1} and the H-N-C=O at 1632 cm^{-1}, all of them representative of the rigid PA segment [21]. The peak at 1086 cm^{-1} was assigned to the C-O-C stretching vibration of the soft PEO segment [45], and at 2935 and 2862 cm^{-1} the symmetric and asymmetric vibration of the C–H bond, respectively [46]. With the addition of ILs, [C_2C_1im][BF_4] and [C_2C_1im][SCN], the characteristic peaks detected at 3155 and 3095 cm^{-1} were assigned to the stretching vibrations of the bond C–H in the imidazole ring [47]. For the CPILM ***M4*** functionalized with [C_2C_1im][BF_4], the peaks at 750 and 520 cm^{-1} were related to the symmetric stretching and the bending vibrations of the B-F bond, respectively. Moreover, the bond C-O-C was red-shifted from 1086 cm^{-1} to lower frequencies at 1049 cm^{-1} [31]. For the thiocyanate-based membrane ***M9***, the characteristic peaks of -C≡S, -C≡N and -S-C≡N appeared at 1165, 1565 and 2055 cm^{-1} [48]. The FTIR spectrum of the TFCMs ***M3***, ***M6***, and ***M9*** revealed the same bands observed in the thick membranes of analogous composition. Moreover, none of the Pebax/IL peaks appeared in the support side (see Fig. S4 of the supplementary information). These facts demonstrate that the selective layers (either Pebax or Pebax/IL) of the TFCMs were successfully deposited over the surface of the porous PVDF support. Likewise, the IL was adequately integrated within the composite selective layer, as the FTIR spectra of the CILPMs and the analogous TFCM with the same composition exhibited the same FTIR profiles.

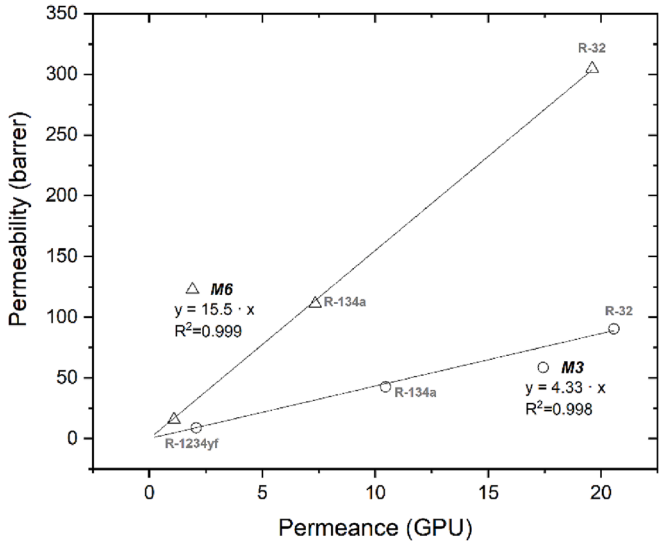

Fig. 3. Indirect estimation of the selective layer thickness of TFCMs from a plot of gas permeability data against gas permeance of TFC-Pebax®1657 (***M3***, ○) and TFC-Pebax®1657/40IL (***M6***, △).

3.2. From lab-scale to large-scale Pebax®1657/IL-TFCMs

The thickness of the membranes fabricated with the conventional solvent casting technique, ***M1*** and ***M4***, was determined in nine different points using a Mitutoyo digital micrometer MDC-25PX (accuracy ± 1 μm), obtaining values of 63 ± 3 and 60 ± 2 μm, respectively. On the other hand, the thickness of the TFCMs was evaluated indirectly from single gas permeation tests as the ratio between the gas permeability in the thick membranes and the gas permeance through the analogous TFCMs, and further confirmed with SEM images.

Fig. 3 illustrates the evaluation of the selective layer thickness of lab-scale TFCMs, from single gas permeation tests at 30 °C and 1.3 bar feed pressure. Table 4 summarizes the background data used to build Fig. 3. Initially, we measured the single gas permeability (*y*-axis) of R-32, R-134a and R-1234yf in experiments with the thick membranes ***M1*** and ***M4***, and the permeance (*x*-axis) of the same gases through the TFCMs ***M3*** and ***M6*** prepared with the spray coating technique by spreading 4 layers of the coating solution onto the PVDF support. The slope of the linear fit for each dataset is considered the effective membrane thickness, which was 4.3 μm for the TFCM of pure Pebax®1657 ***M3***, and 15.5

Table 4
Lab-scale membranes (12.6 cm^2) prepared with pure Pebax®1657 and Pebax®1657/$[C_2C_1im][BF_4]$ 40 wt% with the conventional solvent casting (***M1*** and ***M4***) and spray coating (***M2, M3, M5, M6***) techniques. Permeability values obtained at 30 °C and 1.3 bar feed pressure.

Code	Membrane type	Casting technique	Num. Coating layers	Thickness (μm)	Permeability (barrer)			Permeance (GPU)			Ideal gas selectivity	
					R-1234yf	R-134a	R-32	R-1234yf	R-134a	R-32	R-32/R-1234yf	R-134a/R-1234yf
M1	Neat Pebax®1657	solvent casting	–	63	9.4	42.8	90.1	0.15	0.68	1.43	9.7	4.6
M2	TFC-Pebax®1657	spray-coated	8	9	–	–	–	0.97	4.9	9.9	10.2	5.1
M3	TFC-Pebax®1657	spray-coated	4	5.4	–	–	–	2.24	11.0	21.1	9.4	4.9
M4	Pebax®1657/40%IL	solvent casting	–	60	15.6	110.4	303	0.26	1.84	5.1	19.2	7.0
M5	TFC-Pebax®1657/40%IL	spray-coated	8	38	–	–	–	0.39	2.85	7.9	20.1	7.1
M6	TFC-Pebax®1657/40%IL	spray-coated	4	15.5	–	–	–	1.10	7.3	19.6	17.9	6.7

μm for the TFCM of Pebax®1657-$[C_2C_1im][BF_4]$ (40 wt%) ***M6***. In addition, Figure S5 of the SI shows the SEM images of the cross sections of ***M3*** and ***M6*** TFCMs, from which the average thicknesses were 5.4 ± 0.6 μm and 15.5 ± 1.3 μm, respectively. The SEM values are in good agreement with those obtained in Fig. 3, which validates the characterization of the TFCMs thickness.

Finally, the spray coating technique was also successfully applied onto the porous PVDF supports of higher area (150 cm^2) used in the pilot plant tests. We fabricated three different large scale TFCMs, neat Pebax®1657 (***M7,*** 10.1 ± 2.1 μm), Pebax®1657-$[C_2C_1im][BF_4]$ (40 wt %) (***M8,*** 8.8 ± 1.5 μm) and Pebax®1657-$[C_2C_1im][SCN]$ (40 wt%) (***M9,*** 9.3 ± 1.7 μm). The thickness of the sprayed coated layers was visualized in the SEM images (Fig. 4), in which some penetration of the dense layer is observed in the most superficial part of the pores of the PVDF support. Overall, large defect-free IL-containing membranes with dense layer thicknesses lower than 10 μm were obtained, which were capable of withstanding operating pressures up to 8.5 bar.

3.3. Single and mixed-gas permeation properties of lab-scale TFCMs

This section focuses on the permeation results obtained with the membranes that were tested at laboratory scale. The single gas permeance data of refrigerants R-32, R-134a and R-1234yf through the TFCMs prepared with Pebax®1657 (***M2*** and ***M3***) and Pebax®1657/40% IL (***M5*** and ***M6***) are collected in Table 4. As expected, gas permeance followed the order R-32 > R-134a > R–1234yf, and the TFCMs exhibited superior performance, i.e., higher permeance, as the thickness of the selective layer decreased. In particular, the spray coating of four selective layers increased 15-fold the permeance of the three F-gases, in good agreement with the reduction achieved in the selective layer thickness, from the 63 μm thick sample (***M1***) to the 5.4 μm TFCM (***M3***). Noteworthy, the ideal selectivity for the gas pairs R-32/R-1234yf and R-134a/R-1234yf maintained similar values in the homogeneous thick films and the analogous TFCMs with the same composition. In addition, as a consequence of the solubility changes produced by the IL, the ideal selectivity for target gas pairs was significantly improved: $\alpha_{R32/R1234yf}$ increased 90%, from 9.4 (***M3***) to 17.9 (***M6***), and $\alpha_{R134a/R1234yf}$ increased 37%, from 4.9 (***M3***) to 6.7 (***M6***).

Another consequence of the IL immobilization within the selective layer concerns the effective thickness achieved for the same number of coating layers sprayed over the porous support. For the same number of coating layers (***M5*** relative to ***M2,*** and ***M6*** relative to ***M3***), the gas permeance achieved through the TFCMs that incorporated IL in the selective layer was lower than through the neat Pebax-TFCMs for all gases. This was expected for R-134a and R-1234yf, whose solubility in the composite material decreases with respect to the neat polymer due to unfavorable entropic effects that hinder the absorption of these large molecules into small molar volume ILs, but not for the smallest R-32, whose solubility is enhanced in the presence of the IL $[C_2C_1im][BF_4]$ [24]. Therefore, this effect could be attributed to a higher mass transfer resistance that is likely due to some degree of selective layer penetration into the porous support, a fact that would explain the higher thickness estimated for the IL-based TFCMs.

A whole picture of the progress achieved with the fabrication of defect-free TFCMs is shown in Fig. 5 for one of the most important systems found in novel refrigerants, i.e., the pair R-32 and R-1234yf. As can be seen, for Pebax®1657 membranes (***M1***—***M3***), the R-32 permeance significantly increased (1380%) from the thick membrane (***M1***) to the thinnest TFCM (***M3***), while the ideal R-32/R-1234yf selectivity remained fairly constant. For the Pebax®1657/40%IL membranes, the same effects are observed, i.e., the gas permeance increased (284%), and the ideal gas selectivity remained constant, as the thickness of the selective layer decreased from the CILPM ***M4*** to the TFCMs ***M5*** and ***M6***. Overall, the synergy of reducing the selective layer thickness and functionalizing the polymer material with selective ILs can be observed

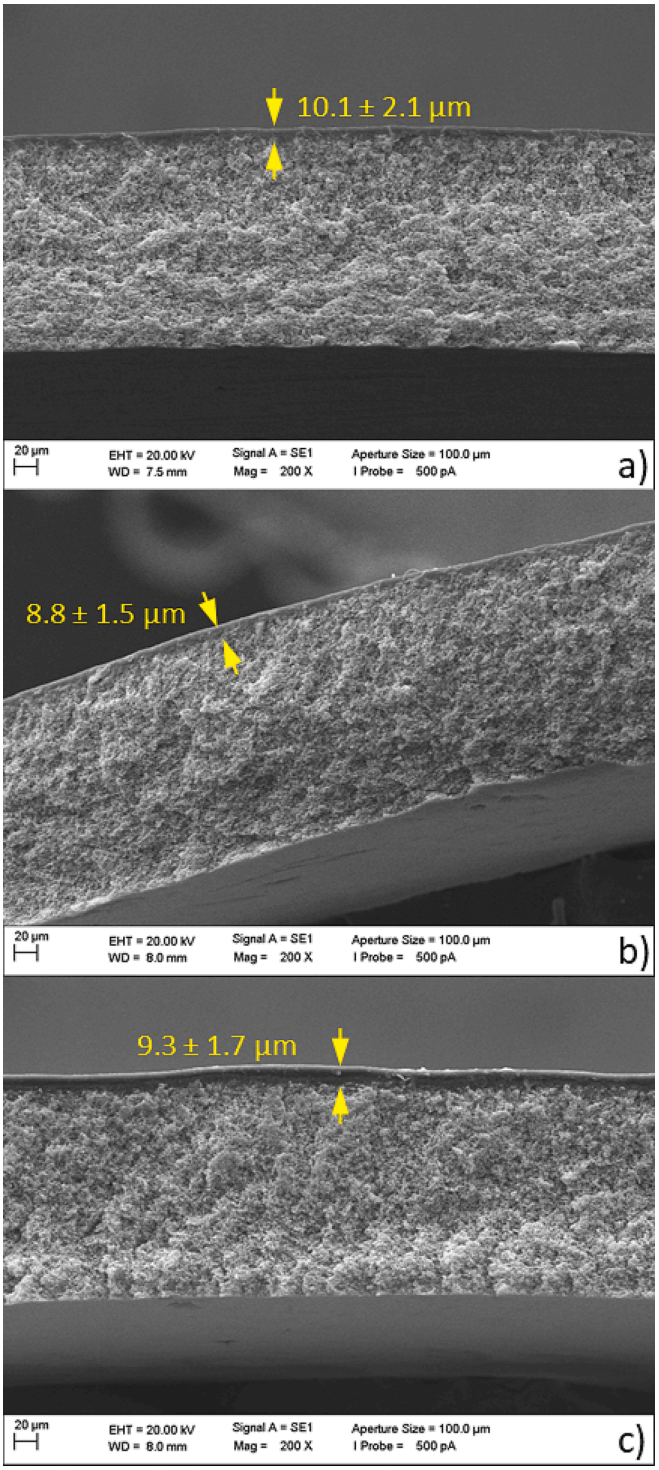

Fig. 4. SEM images of cross-section of the TFCM used in the pilot plant experiments. The dense selective layers are: a) Neat Pebax®1657 (***M7***), b) CILPM Pebax®1657 / 40 wt% $[C_2C_1im][BF_4]$ (***M8***) and c) CILPM Pebax®1657 / 40 wt % $[C_2C_1im][SCN]$ (***M9***). Porous PVDF was used as support.

comparing thick polymer membrane ***M1*** and the IL-based TFCM ***M6,*** the R-32 permeance increased 1271% due to the reduction of the selective layer thickness, and the R-32/R-1234yf ideal selectivity increased 85% thanks to the addition of 40 wt% IL. These findings highlight the need of dedicating more research efforts to improve the casting techniques in order to fabricate competitive defect-free IL-based membranes with thinner selective layers.

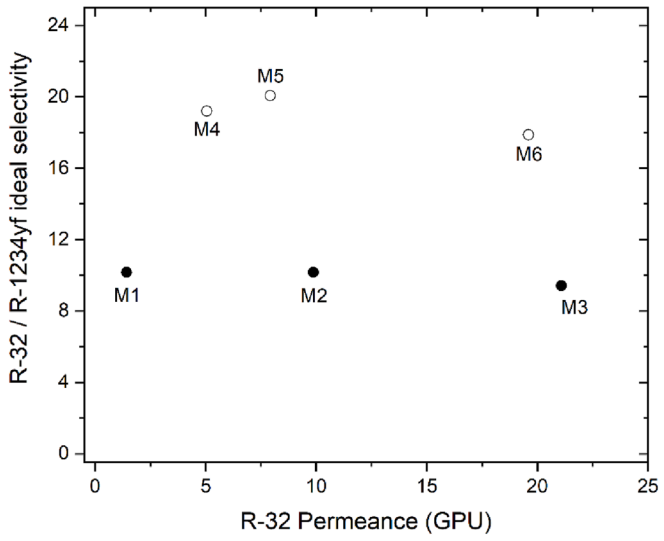

Fig. 5. Ideal R-32/R-1234yf selectivity as a function of membrane type: neat Pebax®1657 (***M1***), TFCM-Pebax (***M2*** and ***M3***), CILPM Pebax®1657/40 wt% $[C_2C_1im][BF_4]$ (***M4***), TFCM- Pebax®1657/40 wt% $[C_2C_1im][BF_4]$(***M5*** and ***M6***). Data obtained at 1.3 bar feed pressure and 30 °C.

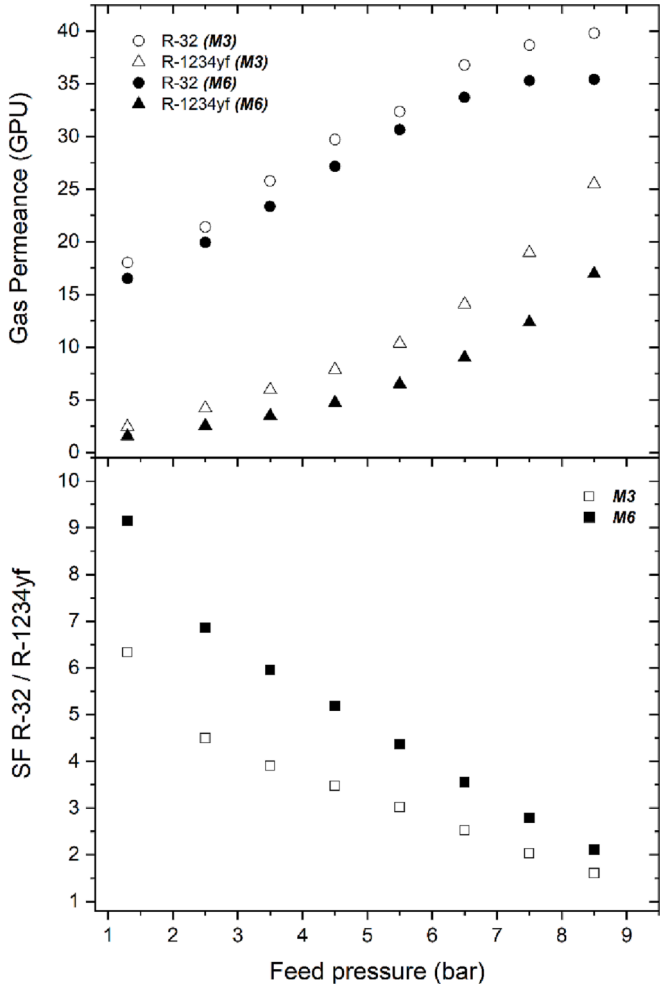

Fig. 6. Separation of mixture R-454B at lab scale: (a) Mixed-gas permeance of R-32 (○) and R-1234yf (Δ), and (b) R-32/R-1234yf competitive selectivity as a function of R-454B feed pressure (1.3–8.5 bar) through the TFCM-Pebax (**M3**, open symbols) and the TFCM-Pebax®1657/40 wt% $[C_2C_1im][BF_4]$ (***M6***, filled symbols). Feed flowrate: 20 cm^3_{STP} min^{-1}. Temperature: 30 °C.

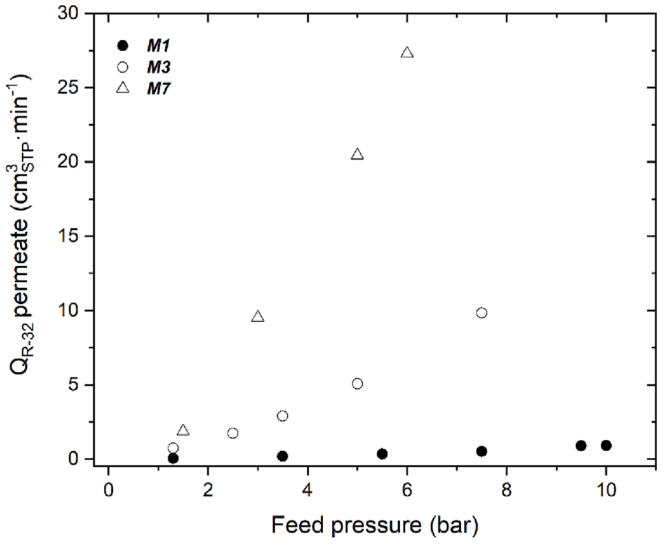

Fig. 7. R-32 flowrate in the permeate as a function of feed pressure for the separation of R-410A refrigerant blend. Membranes compared are all made of neat Pebax®1657: thick membrane at laboratory scale (***M1*** ●), TFCM at laboratory scale (***M3*** ○) and TFCM at pilot plant scale (***M7*** △).

Next, the separation performance of the TFCMs was assessed under relevant pressure and mixed gas feed conditions. To that end, two refrigerant blends that include R-32 in their composition were selected: (1) R-454B, a newly commercialized HFC/HFO mixture (82.9:17.1 mol % R-32 and R-1234yf) (GWP = 466); and (2) R-410A an equimass mixture of R-32 and R-125 (GWP = 2088). Collecting R-410A from end-of-life equipment is regarded as secondary source of R-32, which can be reused for the formulation of new HFC/HFO mixtures. Tables S4 and S5 of the SI present the whole collection of experimental results and the most relevant findings are detailed below.

Fig. 6 shows the gas permeance results achieved when feeding R-454B as a function of the feed pressure (1.3–8.5 bar). As can be seen, the permeances of R-32 and R-1234yf sharply increased with the feed pressure, following the same trend in both TFCMs made of Pebax (***M3***) and Pebax/40% IL composites (***M6***). This pressure-dependence permeance can be attributed to a significant plasticizing behavior of the membrane material due to the highly condensable nature of the refrigerant gases [49,50]. As a result of this effect, the enhancement of R-1234yf permeance at higher pressure was more significant than that observed for R-32, and consequently, the separation factor gradually decreased at increasing pressure.

Similarly, Figure S6 shows the mixed-gas permeance of R-32 and R-125 and the resulting separation factor as a function of R-410A feed pressure through the same TFCMs. The pressure-dependence behavior of the mixed-gas permeance and the separation factor is comparable to that described in the previous case study. That is, an increase of the permeance of both gases, which is more significant for the least permeable gas R-125, and a 77% decrease of the resulting competitive selectivity between 1.3 and 9.5 bar. These results evidence the trade-off between gas permeance and separation factor of the prepared TFCMs for separating fluorinated hydrocarbon mixtures under high pressures relative to their vapor pressure, and reinforce the need for assessing the real separation performance of novel membrane materials under relevant pressure and composition conditions.

Table 5
Experiments performed at pilot plant scale for the separation of R-410A blend (69.8 mol % R-32, 30.2 mol % R-125). Room temperature T = 20 ± 1 °C, feed flowrate = 50 $cm^3_{stp} \cdot min^{-1}$, without sweep gas in the permeate stream.

Code	TFCM composition	Thickness (μm)	Feed Pressure (bar)	Stage cut (%)	R-32 recovery (%)	R-32 Permeate composition (% mol)	R-32 Retentate composition (% mol)	R-32 Exit partial fugacity gradient (bar)
M7	Neat Pebax®1657	10.1 ± 2.1	1.5	3.04	3.68	84.4	68.2	0.15
			3	22.6	27.3	84.3	65.3	1.02
			5	52.2	58.6	78.3	56.6	1.85
			6	71.0	78.3	76.9	47.8	1.86
M8	Pebax®1657 / 40 wt% $[C_2C_1im][BF_4]$	8.8 ± 1.5	1.5	4.20	5.22	86.7	68.9	0.18
			3	33.0	39.8	84.2	63.2	1.00
			5	58.0	67.8	81.6	52.3	1.65
			6	76.0	86.2	79.1	44.2	1.66
M9	Pebax®1657 / 40 wt% $[C_2C_1im][SCN]$	9.3 ± 1.7	1.5	1.00	1.29	89.6	68.6	0.14
			3	18.8	25.2	88.5	64.8	1.05
			5	42.4	53.4	88.2	57.1	2.09
			6	46.8	64.3	87.2	51.9	2.47

Table 6
Experiments performed at pilot plant scale for the separation of R-454B blend (82.9 % mol R-32, 17.1 % mol R-1234yf). Room temperature T = 20 ± 1 °C, feed flowrate = 50 $cm^3_{stp} \cdot min^{-1}$, without sweep gas in the permeate stream.

Code	TFCM composition	Thickness (μm)	Feed Pressure (bar)	Stage cut (%)	R-32 recovery (%)	R-32 Permeate composition (% mol)	R-32 Retentate composition (% mol)	R-32 Exit partial fugacity gradient (bar)
M8	Pebax®1657 / 40 wt% $[C_2C_1im][BF_4]$	8.8 ± 1.5	1.5	5.0	5.72	94.9	82.1	0.264
			3	32.8	37.2	93.9	78.6	1.32
			5	63.2	70.9	93.0	62.5	2.01
			6	74.2	81.2	90.7	55.4	2.18
M9	Pebax®1657 / 40 wt% $[C_2C_1im][SCN]$	9.3 ± 1.7	1.5	2.8	3.24	95.9	81.6	0.236
			3	22.8	26.2	95.2	79.1	1.32
			5	45.2	51.9	95.1	64.1	2.04
			6	59.0	67.1	94.3	62.9	2.54

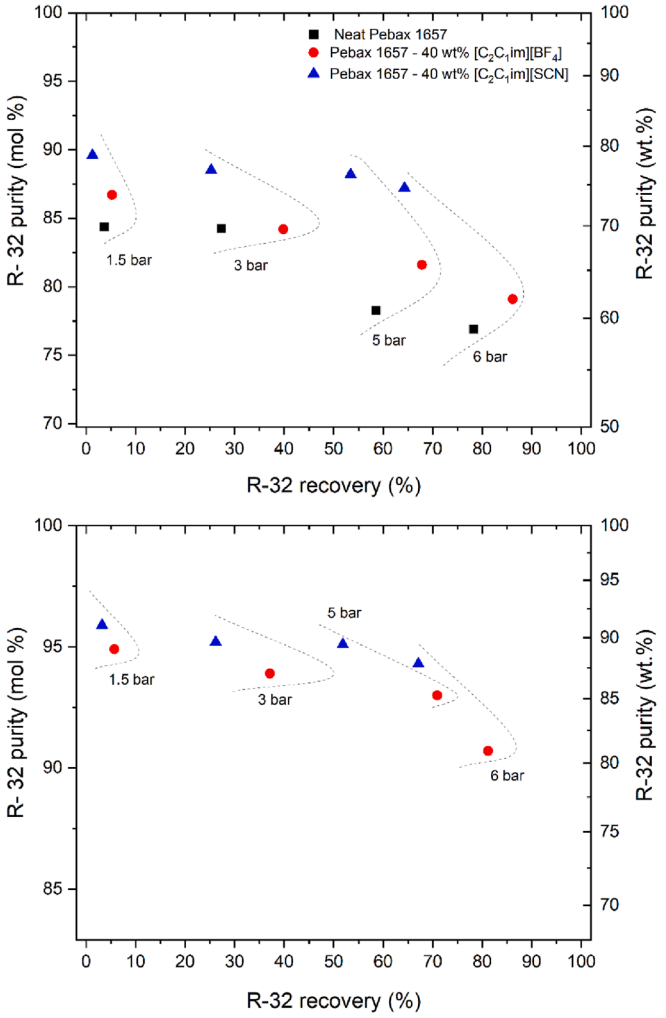

Fig. 8. R-32 concentration in the permeate stream vs. R-32 recovery for the separation of a) R-410A and b) R-454B refrigerant blends. Feed flowrate = 50 cm^3_{STP} min^{-1}, Temperature = 20 ± 1 °C. The TFCMs are: neat Pebax®1657 (***M7***, ■), Pebax®1657-40 wt% [C_2C_1im][BF_4] (***M8***, ●) and Pebax®1657-40 wt % [C_2C_1im][SCN] (***M9***, ▲). The contour lines outline the experimental points carried out at the same feed pressure.

3.4. Tfcms performance at pilot plant scale

Once evaluated the performance of lab-scale TFCMs, the separation of R-410A with a TFCM coated with neat Pebax®1657 dense layer (***M7***) was assessed at pilot scale, and the results compared with the analogous thick film (***M1***) and TFCM (***M3***) lab-scale membranes. Fig. 7 shows the permeation rates of R-32 (Q_{R-32}) through the three membranes. The higher area of ***M7*** significantly increased the permeate flow rate in the pilot plant with respect to the lab-scale membranes ***M1*** and ***M3***. The fact of increasing the permeation area ~ 24 times led to a remarkable increase in permeate flow rate. For instance, at 5 bar feed pressure, R-32 permeate flowrate increased from 4.29 in ***M3*** to 20.4 cm^3_{STP} min^{-1} in ***M7***. At this point, it is worth noting that the pilot plant experiments were performed in the absence of sweep gas in the permeate side, unlike the laboratory scale experiments, a fact that reduced the pressure gradient between both membrane sides in pilot scale experiments.

Next, we tested the performance of the IL-based TFCMs ***M8*** and ***M9*** for separating two feed gas mixtures, R-410A and R-454B, at different feed pressures between 1.5 and 6 bar. Tables 5 and 6 collect the detailed results of stage cut, retentate and permeate compositions, exit driving force (pressure gradient between feed and permeate side) and R-32 recovery (R-410A separation).

Fig. 8 shows the trade-off between the R-32 purity achieved in the permeate stream and the recovery of R-32 at different feed pressures, using contour lines to gather data points obtained at the same feed pressure. The highest R-32 purity in the permeate corresponds to ***M9,*** the TFCM with a selective layer of Pebax®1657-40 wt% [C_2C_1im][SCN]. For instance, in the separation of R-410A (Fig. 8a), R-32 permeate purity ranges from 87.2 to 89.6 mol % for ***M9*** and between 79.1 and 86.7 mol % for ***M8***. In addition, the separation performance of membranes ***M7*** and ***M8*** made of neat Pebax and Pebax functionalized with [C_2C_1im][BF_4], respectively, was negatively affected by increasing the feed pressure, whereas the effect of this operation variable was much less pronounced in the TFCM ***M9*** based on [C_2C_1im][SCN]. The latter behavior facilitates working at higher pressures to increase the recovery of R-32. In contrast, R-32 recovery is higher with the Pebax®1657 / [C_2C_1im][BF_4] TFCM (***M8***). The fact that the selective layer thickness of both membranes is similar further confirmed our previous observations regarding the influence of the IL anion on gas permeability and gas pair selectivity. Enthalpic effects (i.e., hydrogen bonding ability) favors the solubility of fluorinated hydrocarbons in [C_2C_1im][BF_4], and thus lead to an increase in gas permeability. On the other hand, the lower molar volume and absence of fluorine atoms of [C_2C_1im][SCN] hinder the absorption of large fluorocarbons and favors the separation of the smallest R-32 from larger hydrofluorocarbons [8,51].

Overall, the maximum purity of R-32 in the permeate was 89.6 and 95.9 mol %, for the separation of R-410A and R-454B mixtures,

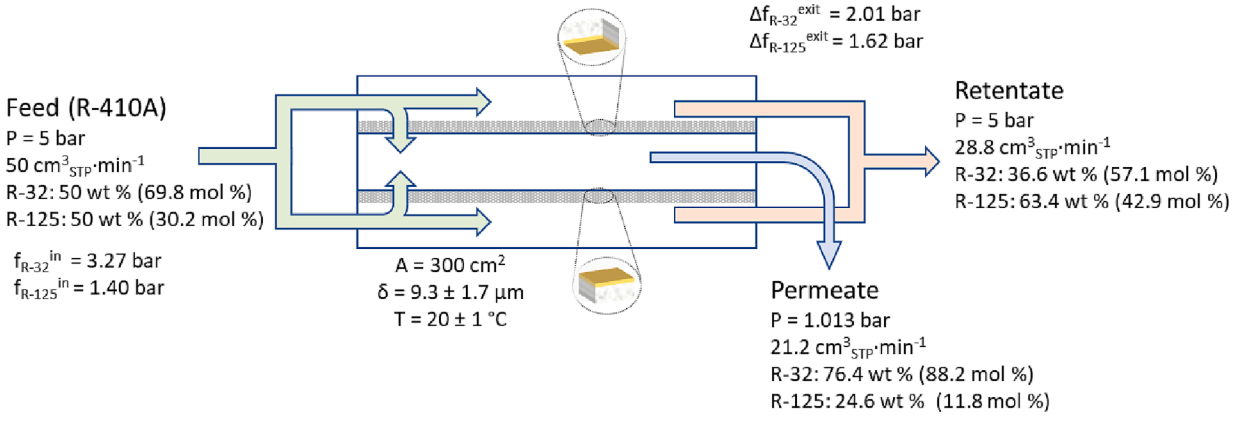

Fig. 9. Mass balance of the separation of the R-410A refrigerant blend in the pilot plant at 5 bar feed pressure with TFCM Pebax®1657/40 wt% [C_2C_1im][SCN] (***M9***).

respectively, at 1.5 bar of feed pressure, yet with low recoveries of 1.3 and 3.2%. However, increasing the feed pressure up to 5 bar resulted in a moderate decrease of the R-32 concentration in the permeate, 88.2 mol % for R-410A separation and 95.1 mol % for R-454B separation, and markedly increased the R-32 recovery, around 52–53% for both feed mixtures. As a final example, Fig. 9 shows the mass balance and compositions of the feed, permeate and retentate streams corresponding to a pilot plant experiment performed at 5 bar with the [C_2C_1im][SCN]-based TFCM ***M9***.

4. Conclusions

The combination of some ionic liquids, such as [C_2C_1im][BF_4] and [C_2C_1im][SCN], with the copolymer Pebax®1657 has proved to be an innovative approach for the recovery of the value-added refrigerant R-32 from azeotropic or close-boiling refrigerant mixtures, like R-410A and R-454B, using membrane technology. However, the development of this type of composite materials for gas separation still remains at laboratory scale. Hence, in the present work, we have taken a step forward towards achieving high-permeate flux membranes with polymer/IL selective skins. Defect-free TFCMs were fabricated using a simple and reliable spray-coating technique at lab-scale (12.6 cm^2). The TFCMs containing up to 40 wt% IL content were stable under relevant pressure conditions so the methodology was adapted to fabricate larger membranes to be tested in a pilot set-up of 300 cm^2. The recovery of R-32 from refrigerant mixtures was assessed with two large scale TFCMs and the best results in terms of R-32 purity and recovery were obtained with the Pebax®1657-40 wt% [C_2C_1im][SCN] TFCM at the highest pressure tested. These results are encouraging for the application of polymer/IL TFCMs in gas separations as there is still plenty of room to improve the coating technique to fabricate membranes with ultra-thin composite selective layers.

CRediT authorship contribution statement

Fernando Pardo: Investigation, Formal analysis, Writing – original draft, Supervision. **Sergio V. Gutiérrez-Hernández:** Investigation, Formal analysis, Writing – original draft. **Paula Rodríguez-San Miguel:** Investigation. **Gabriel Zarca:** Conceptualization, Methodology, Funding acquisition, Writing – review & editing, Supervision. **Ane Urtiaga:** Conceptualization, Methodology, Funding acquisition, Writing – review & editing, Supervision, Project administration.

Declaration of Competing Interest

The authors declare that they have no known competing financial interests or personal relationships that could have appeared to influence the work reported in this paper.

Data availability

Experimental data are provided in the Supplementary Material file. Authors will provide any other data on request

Acknowledgements

This research is supported by Project KET4F-Gas – SOE2/P1/P0823, Project PID2019-105827RB-I00 funded by MCIN/AEI/10.1039/501100011033 (Spain), and project LIFE4F-Gases (LIFE20CCM/ES/001748) co-funded by the European Union LIFE programme. F.P. acknowledges the post-doctoral fellowship (IJC2020-043134-I, 'Juan de la Cierva Incorporación') funded by the Spanish Ministry of Science and Innovation MCIN/AEI/10.13039/501100011033 and the European Union NextGenerationEU/PRTR. S. V. G. acknowledges the pre-doctoral fellowship FPI PRE2020-093568, funded by the Spanish Ministry of Science and Innovation MCIN/AEI/10.13039/501100011033 and by "ESF Investing in your future".

Appendix A. Supplementary data

Supplementary data to this article can be found online at https://doi.org/10.1016/j.seppur.2023.124115.

References

[1] E.J. García, D. Bahamon, L.F. Vega, Systematic Search of Suitable Metal-Organic Frameworks for Thermal Energy-Storage Applications with Low Global Warming Potential Refrigerants, ACS Sustain. Chem. Eng. 9 (2021) 3157–3171, https://doi.org/10.1021/acssuschemeng.0c07797.
[2] H.S. Laine, J. Salpakari, E.E. Looney, H. Savin, I.M. Peters, T. Buonassisi, Meeting global cooling demand with photovoltaics during the 21st century, Energ. Environ. Sci. 12 (2019) 2706–2716, https://doi.org/10.1039/C9EE00002J.
[3] L.F. Lepre, D. Andre, S. Denis-Quanquin, A. Gautier, A.A.H. Pádua, M. Costa Gomes, Ionic Liquids Can Enable the Recycling of Fluorinated Greenhouse Gases, ACS Sustain. Chem. Eng. 7 (2019) 16900–16906, https://doi.org/10.1021/acssuschemeng.9b04214.
[4] M.O. McLinden, M.L. Huber, (R)Evolution of Refrigerants, J. Chem. Eng. Data 65 (2020) 4176–4193, https://doi.org/10.1021/acs.jced.0c00338.
[5] Y. Heredia-Aricapa, J.M. Belman-Flores, A. Mota-Babiloni, J. Serrano-Arellano, J. J. García-Pabón, Overview of low GWP mixtures for the replacement of HFC refrigerants: R134a, R404A and R410A, Int. J. Refrig 111 (2020) 113–123, https://doi.org/10.1016/j.ijrefrig.2019.11.012.
[6] A. Mota-Babiloni, P. Makhnatch, Predictions of European refrigerants place on the market following F-gas regulation restrictions, Int. J. Refrig 127 (2021) 101–110, https://doi.org/10.1016/j.ijrefrig.2021.03.005.
[7] G. Morrison, M.O. McLinden, Azeotropy in refrigerant mixtures: Azéotropie dans les mélanges de frigorigènes, Int. J. Refrig 16 (1993) 129–138, https://doi.org/10.1016/0140-7007(93)90069-K.
[8] S. Asensio-Delgado, F. Pardo, G. Zarca, A. Urtiaga, Enhanced absorption separation of hydrofluorocarbon/hydrofluoroolefin refrigerant blends using ionic liquids, Sep. Purif. Technol. 249 (2020), 117136, https://doi.org/10.1016/j.seppur.2020.117136.
[9] C.G. Albà, L.F. Vega, F. Llovell, Assessment on Separating Hydrofluoroolefins from Hydrofluorocarbons at the Azeotropic Mixture R513A by Using Fluorinated Ionic Liquids: A Soft-SAFT Study, Ind. Eng. Chem. Res. 59 (2020) 13315–13324, https://doi.org/10.1021/acs.iecr.0c02331.
[10] S. Asensio-Delgado, D. Jovell, G. Zarca, A. Urtiaga, F. Llovell, Thermodynamic and process modeling of the recovery of R410A compounds with ionic liquids, Int. J. Refrig 118 (2020) 365–375, https://doi.org/10.1016/j.ijrefrig.2020.04.013.
[11] E.A. Finberg, M.B. Shiflett, Process Designs for Separating R-410A, R-404A, and R-407C Using Extractive Distillation and Ionic Liquid Entrainers, Ind. Eng. Chem. Res. (2021), https://doi.org/10.1021/acs.iecr.1c02891.
[12] A.R.C. Morais, A.N. Harders, K.R. Baca, G.M. Olsen, B.J. Befort, A.W. Dowling, E. J. Maginn, M.B. Shiflett, Phase Equilibria, Diffusivities, and Equation of State Modeling of HFC-32 and HFC-125 in Imidazolium-Based Ionic Liquids for the Separation of R-410A, Ind. Eng. Chem. Res. 59 (2020) 18222–18235, https://doi.org/10.1021/acs.iecr.0c02820.
[13] M.B. Shiflett, A. Yokozeki, Separation of difluoromethane and pentafluoroethane by extractive distillation using ionic liquid, Chimica Oggi-chemistry Today 24 (2006) 28–30.
[14] J.E. Sosa, R. Santiago, D. Hospital-Benito, M. Costa Gomes, J.M.M. Araújo, A. B. Pereiro, J. Palomar, Process Evaluation of Fluorinated Ionic Liquids as F-Gas Absorbents, Environ. Sci. Tech. 54 (2020) 12784–12794, https://doi.org/10.1021/acs.est.0c05305.
[15] E.A. Finberg, T.L. May, M.B. Shiflett, Multicomponent Refrigerant Separation Using Extractive Distillation with Ionic Liquids, Ind. Eng. Chem. Res. 61 (2022) 9795–9812, https://doi.org/10.1021/acs.iecr.2c00937.
[16] J.E. Sosa, C. Malheiro, R.P. Ribeiro, P.J. Castro, M.M. Piñeiro, J.M. Araújo, F. Plantier, J.P. Mota, A.B. Pereiro, Adsorption of fluorinated greenhouse gases on activated carbons: evaluation of their potential for gas separation, J. Chem. Technol. Biotechnol. 95 (2020) 1892–1905, https://doi.org/10.1002/jctb.6371.
[17] D.J.A. Wanigarathna, J. Gao, T. Takanami, Q. Zhang, B. Liu, Adsorption Separation of R-22, R-32 and R-125 Fluorocarbons using 4A Molecular Sieve Zeolite, ChemistrySelect 1 (2016) 3718–3722, https://doi.org/10.1002/slct.201600689.
[18] J.E. Sosa, C. Malheiro, P.J. Castro, R.P.P.L. Ribeiro, M.M. Piñeiro, F. Plantier, J.P. B. Mota, J.M.M. Araújo, A.B. Pereiro, Exploring the Potential of Metal-Organic Frameworks for the Separation of Blends of Fluorinated Gases with High Global Warming Potential, Global, Challenges n/a (2022) 2200107, https://doi.org/10.1002/gch2.202200107.
[19] D.K.J.A. Wanigarathna, J. Gao, B. Liu, Metal organic frameworks for adsorption-based separation of fluorocompounds: a review, Materials, Advances 1 (2020) 310–320, https://doi.org/10.1039/D0MA00083C.
[20] J.E. Sosa, R.P.P.L. Ribeiro, P.J. Castro, J.P.B. Mota, A.B. Pereiro, J.M.M. Araújo, Sorption of fluorinated greenhouse gases in silica-supported fluorinated ionic liquids, J. Environ. Chem. Eng. 10 (6) (2022) 108580, https://doi.org/10.1016/j.jece.2022.108580.
[21] C. Hermida-Merino, F. Pardo, G. Zarca, J.M.M. Araújo, A. Urtiaga, M.M. Piñeiro, A. B. Pereiro, Integration of Stable Ionic Liquid-Based Nanofluids into Polymer

Membranes. Part I: Membrane Synthesis and Characterization, Nanomaterials 11 (2021) 607, https://doi.org/10.3390/nano11030607.
[22] F. Pardo, S.V. Gutiérrez-Hernández, C. Hermida-Merino, J.M.M. Araújo, M. M. Piñeiro, A.B. Pereiro, G. Zarca, A. Urtiaga, Integration of Stable Ionic Liquid-Based Nanofluids into Polymer Membranes, Part II: Gas Separation Properties toward Fluorinated Greenhouse Gases, Nanomaterials 11 (2021) 582, https://doi.org/10.3390/nano11030582.
[23] F. Pardo, S.V. Gutiérrez-Hernández, G. Zarca, A. Urtiaga, Toward the Recycling of Low-GWP Hydrofluorocarbon/Hydrofluoroolefin Refrigerant Mixtures Using Composite Ionic Liquid-Polymer Membranes, ACS Sustain. Chem. Eng. 9 (2021) 7012–7021, https://doi.org/10.1021/acssuschemeng.1c00668.
[24] F. Pardo, G. Zarca, A. Urtiaga, Separation of Refrigerant Gas Mixtures Containing R32, R134a, and R1234yf through Poly(ether-block-amide) Membranes, ACS Sustain. Chem. Eng. 8 (2020) 2548–2556, https://doi.org/10.1021/acssuschemeng.9b07195.
[25] F. Pardo, G. Zarca, A. Urtiaga, Effect of feed pressure and long-term separation performance of Pebax-ionic liquid membranes for the recovery of difluoromethane (R32) from refrigerant mixture R410A, J. Membr. Sci. 618 (2021), 118744, https://doi.org/10.1016/j.memsci.2020.118744.
[26] A.N. Harders, E.R. Sturd, J.E. Vallier, D.R. Corbin, W.R. White, C.P. Junk, M. B. Shiflett, Selective separation of HFC-32 from R-410A using poly (dimethylsiloxane) and a copolymer of perfluoro(butenyl vinyl ether) and perfluoro(2,2-dimethyl-1,3-dioxole), J. Membr. Sci. 652 (2022), 120467, https://doi.org/10.1016/j.memsci.2022.120467.
[27] A.N. Harders, E.R. Sturd, L. Wallisch, H. Schmidt, Y. Mendoza-Apodaca, D. R. Corbin, W. White, C.P. Junk, M.B. Shiflett, Solubility, Diffusivity, and Permeability of HFC-32 and HFC-125 in Amorphous Copolymers of Perfluoro (butenyl vinyl ether) and Perfluoro(2,2-dimethyl-1,3-dioxole), Ind. Eng. Chem. Res. (2023), https://doi.org/10.1021/acs.iecr.2c04518.
[28] S.V. Gutiérrez-Hernández, F. Pardo, A.B. Foster, P. Gorgojo, P.M. Budd, G. Zarca, A. Urtiaga, Outstanding performance of PIM-1 membranes towards the separation of fluorinated refrigerant gases, J. Membr. Sci. 121532 (2023), https://doi.org/10.1016/j.memsci.2023.121532.
[29] P. Bernardo, J.C. Jansen, F. Bazzarelli, F. Tasselli, A. Fuoco, K. Friess, P. Izák, V. Jarmarová, M. Kačírková, G. Clarizia, Gas transport properties of Pebax®/room temperature ionic liquid gel membranes, Sep. Purif. Technol. 97 (2012) 73–82, https://doi.org/10.1016/j.seppur.2012.02.041.
[30] H. Rabiee, A. Ghadimi, T. Mohammadi, Gas transport properties of reverse-selective poly(ether-b-amide6)/[Emim][BF4] gel membranes for CO2/light gases separation, J. Membr. Sci. 476 (2015) 286–302, https://doi.org/10.1016/j.memsci.2014.11.037.
[31] W. Fam, J. Mansouri, H. Li, V. Chen, Improving CO_2 separation performance of thin film composite hollow fiber with Pebax®1657/ionic liquid gel membranes, J. Membr. Sci. 537 (2017) 54–68, https://doi.org/10.1016/j.memsci.2017.05.011.
[32] T. Brinkmann, J. Lillepärg, H. Notzke, J. Pohlmann, S. Shishatskiy, J. Wind, T. Wolff, Development of CO_2 Selective Poly(Ethylene Oxide)-Based Membranes: From Laboratory to Pilot Plant Scale, Engineering 3 (2017) 485–493, https://doi.org/10.1016/J.ENG.2017.04.004.
[33] T. Brinkmann, J. Pohlmann, U. Withalm, J. Wind, T. Wolff, Theoretical and Experimental Investigations of Flat Sheet Membrane Module Types for High Capacity Gas Separation Applications, Chem. Ing. Tech. 85 (2013) 1210–1220, https://doi.org/10.1002/cite.201200238.
[34] X. Jiang, C.Y. Chuah, K. Goh, R. Wang, A facile direct spray-coating of Pebax® 1657: Towards large-scale thin-film composite membranes for efficient CO_2/N_2 separation, J. Membr. Sci. 638 (2021), 119708, https://doi.org/10.1016/j.memsci.2021.119708.
[35] J. Zhou, M.M. Mok, M.G. Cowan, W.M. McDanel, T.K. Carlisle, D.L. Gin, R. D. Noble, High-Permeance Room-Temperature Ionic-Liquid-Based Membranes for CO_2/N_2 Separation, Ind. Eng. Chem. Res. 53 (2014) 20064–20067, https://doi.org/10.1021/ie5040682.
[36] Z. Dai, L. Bai, K.N. Hval, X. Zhang, S. Zhang, L. Deng, Pebax®/TSIL blend thin film composite membranes for CO_2 separation, Science China Chemistry 59 (2016) 538–546, https://doi.org/10.1007/s11426-016-5574-3.
[37] D. Nikolaeva, S. Loïs, P.I. Dahl, M. Sandru, J. Jaschik, M. Tanczyk, A. Fuoco, J. C. Jansen, I.F.J. Vankelecom, Water Vapour Promotes CO_2 Transport in Poly(ionic liquid)/Ionic Liquid-Based Thin-Film Composite Membranes Containing Zinc Salt for Flue Gas Treatment, Appl. Sci. 10 (2020) 3859, https://doi.org/10.3390/app10113859.
[38] S. Nur Alwani Shafie, V. Viriya, N. Abdul Hadi Md Nordin, M. Roil Bilad, M. Dzul Hakim Wirzal, Ionic Liquid Blend Thin Film Composite Membrane for Carbon Dioxide Separation, IOP Conference Series: Materials Science and Engineering 1142 (2021) 012013, https://doi.org/10.1088/1757-899x/1142/1/012013.
[39] H. Seon Bang, S. Jang, Y. Soo Kang, J. Won, Dual facilitated transport of CO_2 using electrospun composite membranes containing Ionic liquid, J. Membr. Sci. 479 (2015) 77–84, https://doi.org/10.1016/j.memsci.2015.01.020.
[40] J. Han, L. Bai, S. Luo, B. Yang, Y. Bai, S. Zeng, X. Zhang, Ionic liquid cobalt complex as O_2 carrier in the PIM-1 membrane for O_2/N_2 separation, Sep. Purif. Technol. 248 (2020), 117041, https://doi.org/10.1016/j.seppur.2020.117041.
[41] G. Huang, A.P. Isfahani, A. Muchtar, K. Sakurai, B.B. Shrestha, D. Qin, D. Yamaguchi, E. Sivaniah, B. Ghalei, Pebax/ionic liquid modified graphene oxide mixed matrix membranes for enhanced CO_2 capture, J. Membr. Sci. 565 (2018) 370–379, https://doi.org/10.1016/j.memsci.2018.08.026.
[42] A. Jomekian, B. Bazooyar, R.M. Behbahani, T. Mohammadi, A. Kargari, Ionic liquid-modified Pebax® 1657 membrane filled by ZIF-8 particles for separation of CO_2 from CH_4, N_2 and H_2, J. Membr. Sci. 524 (2017) 652–662, https://doi.org/10.1016/j.memsci.2016.11.065.
[43] S. Pishva, S. Hassanajili, Investigation on effect of ionic liquid on CO_2 separation performance and properties of novel co-casted dual-layer PEBAX-ionic liquid/PES composite membrane, J. Ind. Eng. Chem. 107 (2022) 180–196, https://doi.org/10.1016/j.jiec.2021.11.046.
[44] N. Daems, S. Milis, R. Verbeke, A. Szymczyk, P.P. Pescarmona, I.F.J. Vankelecom, High-performance membranes with full pH-stability, RSC Adv. 8 (2018) 8813–8827, https://doi.org/10.1039/C7RA13663C.
[45] P. Bernardo, G. Clarizia, Enhancing Gas Permeation Properties of Pebax® 1657 Membranes via Polysorbate Nonionic Surfactants Doping, Polymers 12 (2020) 253, https://doi.org/10.3390/polym12020253.
[46] Y. Qiu, J. Ren, D. Zhao, H. Li, M. Deng, Poly(amide-6-b-ethylene oxide)/[Bmim][Tf2N] blend membranes for carbon dioxide separation, Journal of Energy Chemistry 25 (2016) 122–130, https://doi.org/10.1016/j.jechem.2015.10.009.
[47] S.A. Katsyuba, P.J. Dyson, E.E. Vandyukova, A.V. Chernova, A. Vidiš, Molecular Structure, Vibrational Spectra, and Hydrogen Bonding of the Ionic Liquid 1-Ethyl-3-methyl-1H-imidazolium Tetrafluoroborate, Helv. Chim. Acta 87 (2004) 2556–2565, https://doi.org/10.1002/hlca.200490228.
[48] S.H.K. p, M.S. Thayyil, V.K. Rajan, A. Antony, The Interplay between Charge Transport and CO_2 Capturing Mechanism in [EMIM][SCN] Ionic Liquid: A Broadband Dielectric Study, J. Phys. Chem. B 123 (30) (2019) 6618–6626, https://doi.org/10.1021/acs.jpcb.9b03929.
[49] S.A. Stern, S.M. Fang, R.M. Jobbins, Permeation of gases at high pressures, Journal of Macromolecular Science, Part B 5 (1971) 41–69, https://doi.org/10.1080/00222347108212520.
[50] S.A. Stern, S.-M. Fang, H.L. Frisch, Effect of pressure on gas permeability coefficients. A new application of "free volume" theory, Journal of Polymer Science Part A-2: Polymer Physics 10 (1972) 201–219, https://doi.org/10.1002/pol.1972.160100202.
[51] S. Asensio-Delgado, F. Pardo, G. Zarca, A. Urtiaga, Absorption separation of fluorinated refrigerant gases with ionic liquids: Equilibrium, mass transport, and process design, Sep. Purif. Technol. 276 (2021), 119363, https://doi.org/10.1016/j.seppur.2021.119363.